Received: 17 December 2018 | Accepted: 13 January 2019

DOI: 10.1111/jace.16324

ORIGINAL ARTICLE

Journal of the American Ceramic Society

Amorphous boron suboxide

Murat Durandurdu[1]

Department of Materials Science & Nanotechnology Engineering, Abdullah Gül University, Kayseri, Turkey

Correspondence
Murat Durandurdu, Department of Materials Science & Nanotechnology Engineering, Abdullah Gül University, Kayseri, Turkey.
Email: murat.durandurdu@agu.edu.tr

Funding information
Türkiye Bilimsel ve Teknolojik Araştirma Kurumu, Grant/Award Number: 117M372

Abstract

We study the atomic structure and the electronic and mechanical properties of amorphous boron suboxide (B_6O) using an ab initio molecular dynamic technique. The amorphous network is attained from the rapid solidification of the melt and found to consist of boron and oxygen-rich regions. In the boron-rich regions, boron atoms form mostly perfect or imperfect pentagonal pyramid-like configurations that normally yield the construction of ideal and incomplete B_{12} molecules in the model. In addition to the B_{12} molecules, we also observe the development of a pentagonal bipyramid (B_7) molecule in the noncrystalline structure. In the oxygen-rich regions, on the other hand, boron and oxygen atoms form threefold and twofold coordinated motifs, respectively. The boron-rich and oxygen-rich regions indeed represent structurally the characteristic of amorphous boron and boron trioxide (B_2O_3). The amorphous phase possesses a small band gap energy with respect to the crystal. On the bases of the localization of the tail states, we suggest that the p-type doping might be more convenient than the n-type doping in amorphous B_6O. Bulk modulus and Vickers hardness of the noncrystalline configuration is estimated are be 106 and 13-18 GPa, respectively, which are noticeably less than those of the crystalline structure. Such a noticeable decrease in the mechanical properties is attributed to the presence of open structured B_2O_3 glassy domains in the amorphous model.

KEYWORDS
amorphous, boron suboxide, hardness

1 | INTRODUCTION

Boron suboxide (B_6O) has been of substantial scientific attention since it offers a wide range of extraordinary physical and chemical properties. Lightweight, high hardness, high thermal conductivity, high chemical inertness etc. are some of its great features.[1–6] B_6O is considered as a superhard material having a Vickers hardness of 38-45 GPa,[7–9] which is comparable with that of B_4C and cubic BN.[5] Indeed B_6O is ranked to be the third hardest material. Yet it has not been commercialized because it is a typical unsinterable material under ambient pressure condition.[10,11] A proper sintering agent has not been established since B_6O is simply oxidized to form B_2O_3.[10,11] Furthermore its full densification is quite challenging even by high-pressure sintering techniques.[10,11]

B_6O is generally synthesized by the chemical interaction of amorphous or crystalline boron phases with B_2O_3 or other oxidants[12–18] at high temperature and pressure conditions ranging from ambient to 8 GPa.[2,15,19–22] However, the samples fabricated at ambient pressure present usually oxygen-deficiency B_6O_x ($x < 0.9$) and a rather poor crystallinity.[15] The production of stoichiometric B_6O can be achievable at pressures exceeding 4.0 GPa and temperatures of around 2000 K if the amorphous B is used as a starting structure.[2] Yet, later investigation has shown that stoichiometric B_6O can be fabricated at a pressure as low as 1.0 GPa if β-B_{106} crystal is used as a starting material.[23] Nonetheless, a pure phase of B_6O is still challenging to manufacture. B_6O has a crystal structure related to α-rhombohedral boron,[3,16] which consists the quasimolecular (B_{12}) icosahedron and two oxygen (O–O) atom chains at the center of the rhombohedron.

Amorphous boron oxide (BO_x) films including B_6O can be produced using distinctive experimental techniques such as evaporation, cathodic arc deposition, and radio frequency magnetron sputtering.[24–30] These experimental studies mainly focused the mechanical properties of the thin films and proposed that an increase in O concentration and a decrease film density lead to a decrease in the mechanical properties.

There have been two theoretical attempts to model amorphous BO_x. In the classical molecular dynamics simulations,[25] the influence of O content on the mechanical properties was explored and it was reported that B–O bonds promoted ionicity rendering a lower elastic modulus with increasing O concentration. In the second study,[31] the effect of impurities (N, C, Ar etc.) on the mechanical properties of BO_x films was investigated using ab initio simulations.

In a high-pressure study,[32] during pressure release, the B_6O crystal was found to transform to an amorphous state consisting of the amorphous boron trioxide (a-B_2O_3) and glassy boron (a-B). Additionally during the nanoindentation process,[33] a shear-induced local amorphization of B_6O was perceived in the experimental study and it was inspected in an ab initio simulation.[34]

These experimental studies expose the fact that amorphous B_6O (a-B_6O) can be straightforwardly obtainable under different conditions but no serious theoretical investigation has been executed to disclose its atomic structure and its electrical and mechanical properties. The main purpose of the present work is to generate a-B_6O using an ab initio molecular dynamics (AIMD) approximation and to provide information about it in details.

2 | METHOD

The present AIMD simulations were carried out by the SIESTA code[35] within the pseudopotential approach[36] and generalized gradient approximation (GGA).[37,38] The DZ basis sets and sole Γ point for the Brillion zone integration were selected. Constant number of atom, pressure, and temperature ensemble was chosen to execute the AIMD simulations. Temperature and pressure were controlled by the velocity scaling and the Parrinelo-Rahman[39] algorithms, respectively. The each time step was arranged to be 1.0 fs. Our preliminary structure had a cubic symmetry and consisted of 224 atoms (192 B atoms and 32 O atoms). We applied a temperature of 2500 K to the initial structure for 40 ps. In order to collect data, additional 1000 MD steps were run. In order to see whether the temperature of 2500 K was high enough to produce the dynamics of a liquid state, we calculated the mean square displacement (MSD) shown in Figure 1 As can be seen from the figure, above 130 fs, we had a linear behavior in the MSD and calculated the diffusion constant D from the Einstein relation ($< (r(t)-r(0))^2 > = 6tD$) to be ~1.75×10^{-4} cm^2/s between 200 and 600 fs. We should note here that the melting temperature of B_6O at ambient pressure is not known yet because it decomposes beyond 2030 K.[40] So our liquid state at 2500 K is indeed a hypothetical liquid state of B_6O at zero pressure. Then we reduced temperature gradually from 2500 to 300 K in about 200 ps. Lastly, the structure was optimized until the maximum force was smaller than 0.01 eV/Å. The ISAACS software[41] was employed to acquire some information about the B_6O systems at the atomistic level. The VESTA program[42] was used to visualize the structures.

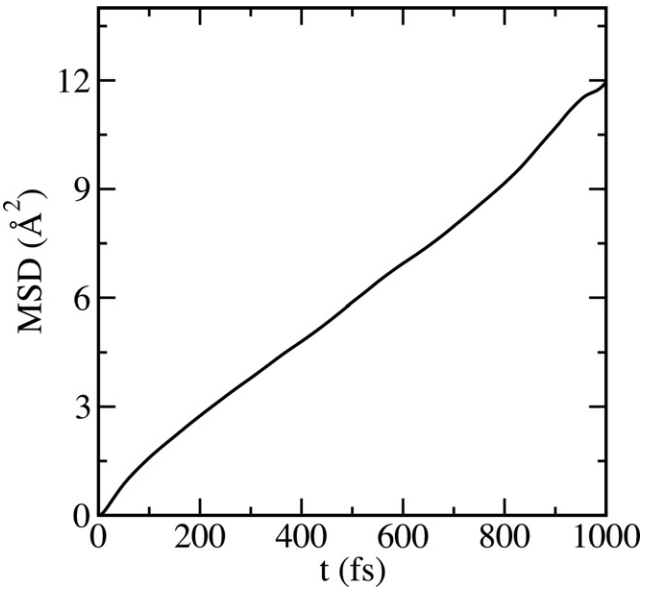

FIGURE 1 Mean square displacement of B_6O at 2500 K

3 | RESULTS

3.1 | Atomic structure

Figure 2 demonstrates the partial pair distribution functions (PPDFs) for a-B_6O, as well as the crystalline B_6O and B_2O_3 structures, which can deliver important information regarding the local structure of materials. An assessment of the B–O and O–O correlation functions discloses radical distinctions between amorphous and crystalline B_6O phases and some resemblances between a-B_6O and the B_2O_3 crystal. The first peak of the B–O partial for the B_6O crystal is placed at 1.51 Å. This value is in good agreement with the previous plane wave simulation result of 1.50 Å[43] but slightly longer than the experimental results of 1.43-1.47 Å.[16,44] On the other hand, the mean B–O distance of a-B_6O is estimated to be 1.37 Å, which is rather shorter than that in the crystal structure (1.51 Å) but it is remarkably comparable with the B–O bond length of 1.35 Å formed in the B_2O_3 crystal. The first

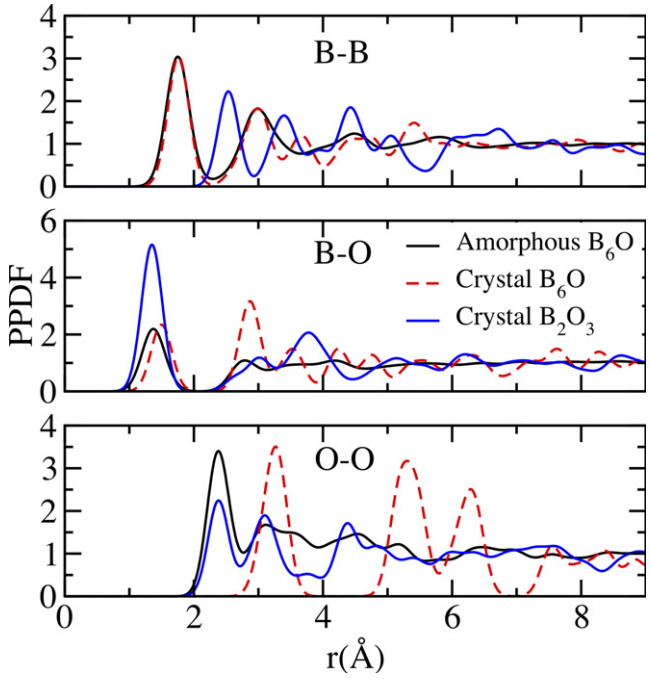

FIGURE 2 Partial pair distribution functions of a-B_6O, the B_6O, and B_2O_3 crystals [Color figure can be viewed at wileyonlinelibrary.com]

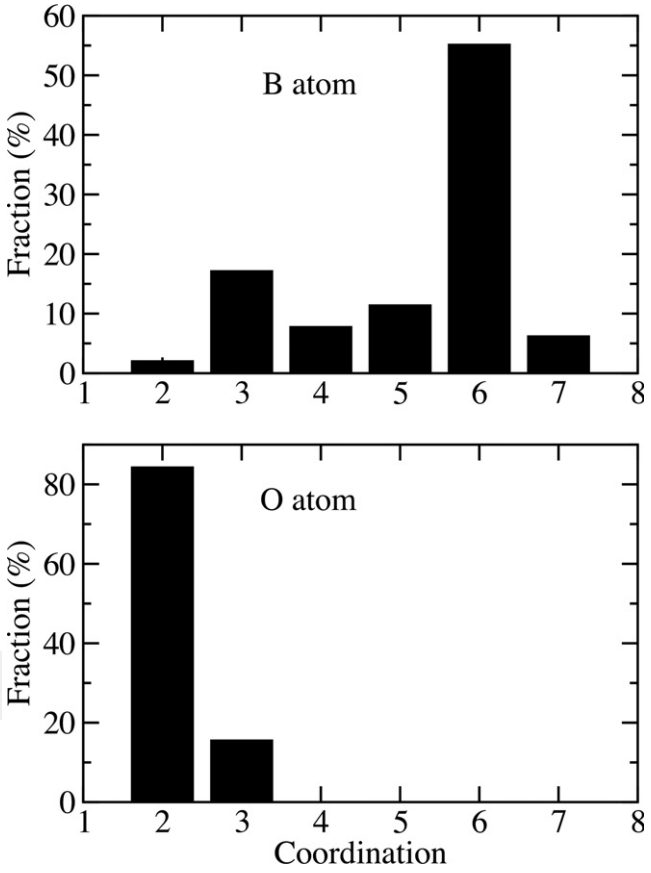

FIGURE 3 Coordination distribution of the amorphous model

O–O peak shifts from 3.35 Å in the crystalline B_6O structure to 2.38 Å in the amorphous form, signifying that O–O packing in these two B_6O phases is quite different. On the other hand, the value obtained for the noncrsytalline state is exactly equal to the one predicted for the B_2O_3 crystal (Figure 2). The shortening of B–O and O–O pair correlations to those of B_2O_3 suggests the onset of polymerization of B–O units in the computer generated a-B_6O network. The mean B–B bond length estimated for a-B_6O is 1.75 Å, which does indeed accord with the theoretical values of 1.70-1.81 Å[43] and the experimental predictions of 1.68-1.83 Å[16] in the B_6O crystal (the different B–B bond distances in the crystal is due to the intericosahedral and intraicosahedral bonds). The second and third peaks of the B–B pair are located at 2.98 and 4.48 Å, correspondingly. The position of first two peaks of the B–B correlation is quite close to 1.76 and 2.99 Å projected for the crystalline B_6O phase while that of the third one is reasonably off from 3.66 Å produced in the crystal. The location of first three peaks is also parallel to 1.80 Å (1.78 Å), 2.93 Å (3.15 Å) and 4.38 Å (4.7 Å) reported for a-B (liquid B at 2600 K) in experimental studies[45,46] and 1.78, 3.02 and 4.54 Å produced for an a-B model generated using an ab initio simulation.[47] It should be noted the noticeable second and third peaks in the B–B pairs, indicating the formation of a medium range order in a-B_6O, which is possibly associated with the presence of ideal or defective pentagonal pyramids and B_{12} icosahedral molecules in the amorphous network. The most important outcome of the PPDFs analyses is that the amorphous B_6O model carries structurally some features of both B_2O_3 system and a-B.

In order to determine coordination number and distribution for each species, we use radii of 2.1 and 2.6 Å, which are the first minimum of the B–B and B–O correlation functions, respectively. The coordination distribution of the amorphous model is offered in Figure 3. From the figure, one can perceive that B coordination ranges from two to seven and the sixfold coordination is the most dominant one with a fraction of about 55%. The second and third dominant ones are threefold (17%) and fivefold (11%) coordinations, respectively. This distribution yields a mean coordination number of B atoms to be about 5.2, which is comparable with 6 formed in the crystal. For the O atoms, on the other hand, twofold coordination is the most privilege one with the frequency of 84%. The fraction of threefold coordination is about 16%. The average coordination number of O atoms is 2.15, which is 3 in the B_6O crystal. On the basis of the coordination analysis, we conclude that the environment of O atoms in the amorphous state is significantly different than that of O atoms in the crystalline B_6O structure but might be similar to one formed in the B_2O_3 crystal (or glass) since they consist of twofold coordinated O atoms.

In order to identify the types of clusters formed around B atoms, we use the Voronoi polyhedra approach.[48] Voronoi polyhedrons are represented by the indices $\langle n_3, n_4, n_5, n_6, \ldots \rangle$, where n_i and $\sum n_i$ represent the number of i-edge faces of a polyhedron and the coordination number, correspondingly. In the crystalline B_6O phase, there is only one type of polyhedron that is represented by the $< 2, 2, 2, 0 >$ index and as expected it is the ideal pentagonal pyramid-like clusters. On the other hand, we identify nine different polyhedrons for B atoms in the amorphous configuration and the most dominant ones are characterized by the $< 2, 2, 2, 0 >$ (53%), and $< 2, 3, 0, 0 >$ (10%) indices. Here, the $< 2, 3, 0, 0 >$ type polyhedron corresponds to incomplete pentagonal pyramid-like structures. These two type clusters cause the construction of perfect and imperfect B_{12} icosahedrons in the boron reach regions in the noncrsytalline network. From the visualization of the model, we also detect the development of a pentagonal bipyramidal type of cluster (B_7) in a-B_6O (Figure 4).

The amorphous model is further evaluated by the bond angle distribution functions to have additional knowledge about its local structure at the atomistic level. Figure 5 shows the distribution of angles and reveals severe distinctions about the local structure of the amorphous and crystalline phases. The most obvious one is the presence of O–B–O angles in the amorphous model contrary to the crystal. The occurrence of these angles provides additional support for the polymerization of B–O units in the noncrystalline configuration while such units are isolated in the crystal. The O–B–O distribution ranges from 100° to 130° and has two leading peaks at 115° and 120°. Also the B–O–B angles have a large distribution ranging from 95° to 170° while these angles produce a sole peak at 120° for the crystal. The B–B–B distribution of noncrsytalline model, on the other hand, has two main peaks at around 60° and 108° similar to the B_6O crystal. These peaks are produced by the intraicosahedral bonds of the pentagonal pyramids. The sharp peak around 123° is generated by intericosahedral units in the crystal. Such a peak is weakly presented in a-B_6O because the ideal or incomplete pentagonal pyramid-like units are randomly linked to each other.

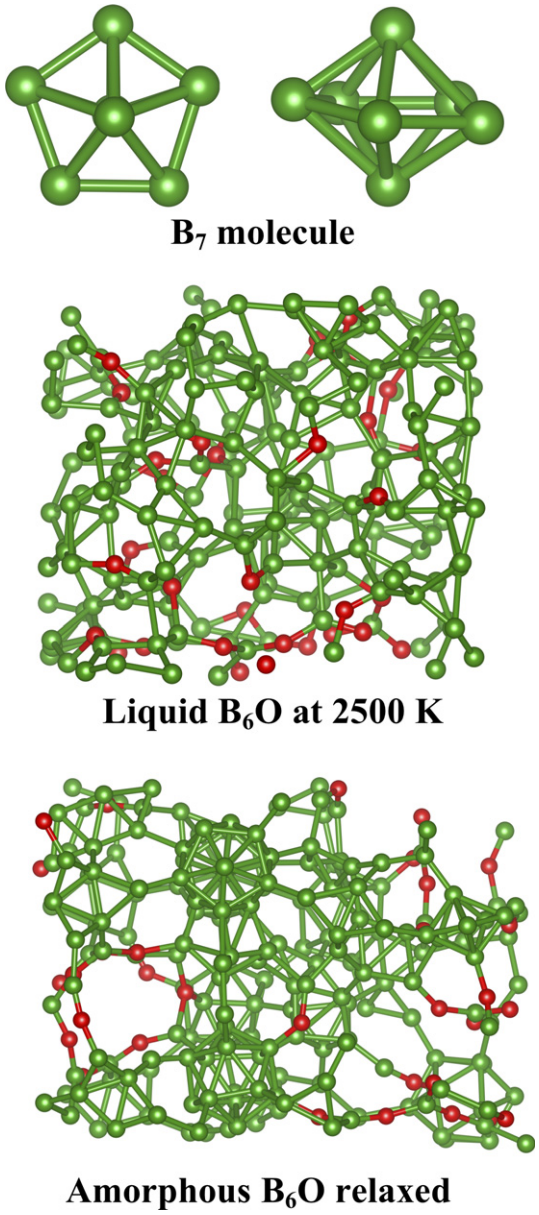

FIGURE 4 Pentagonal bipyramidal type of cluster (B_7) in the amorphous network. Liquid state at 2500 K and a-B_6O [Color figure can be viewed at wileyonlinelibrary.com]

3.2 | Electrical properties

The electronic structure of the B_6O phases is analyzed by the total density of states (TDOS), partial density of state (PDOS), and inverse participation ratio $(\mathrm{IPR}(\psi_j) = N\sum_{i=1}^{N} a_i^{k4} / \left(\sum_{i=1}^{N} a_i^{k2}\right)^2$ where $\psi_k = \sum_{i=1}^{N} a_i^k \phi_i$ is the kth eigenstate and N is the number of atoms[49]). The computed TDOS for both crystalline and amorphous states are provided in Figure 6. The HOMO-LUMO band gap energy for the B_6O crystal is 2.47 eV in good agreement with the earlier first principles GGA simulation results of 1.9-2.4 eV.[50,51] This value however is <2.93-3.0 eV estimated using the G_0W_0 approximation.[51,52] For the amorphous state, the HOMO-LUMO band gap energy is fairly small and about 0.51 eV. Since the gap energy of the crystal is underestimated about a factor of ~1.2, relative to the G_0W_0 approximation, we speculate here that a-B_6O would have about 0.6 eV band gap energy. The PDOS analysis of both forms of B_6O reveals that B-p states are dominant for both valance and

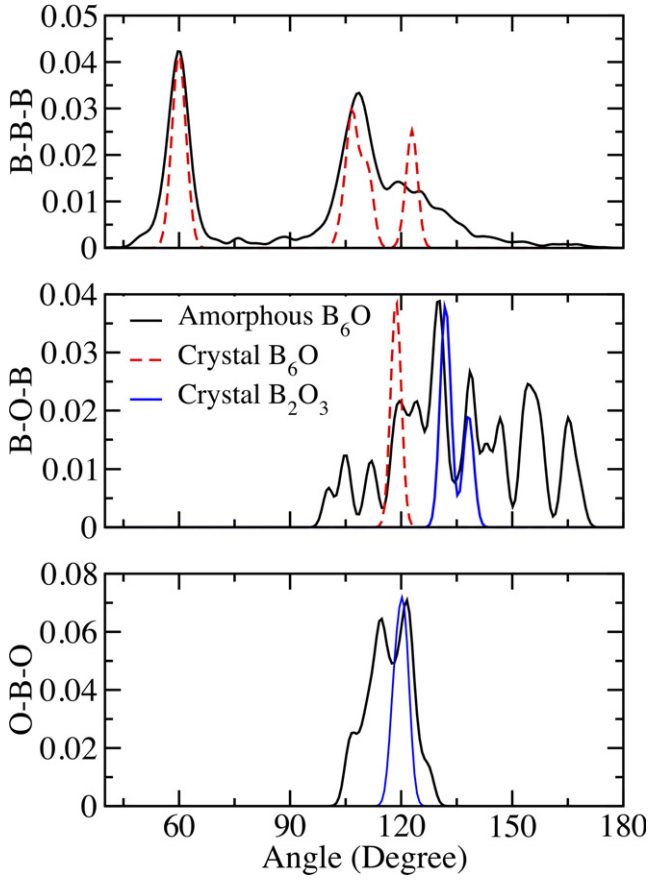

FIGURE 5 Bond angle distribution functions of a-B_6O, B_6O, and B_2O_3 crystals [Color figure can be viewed at wileyonlinelibrary.com]

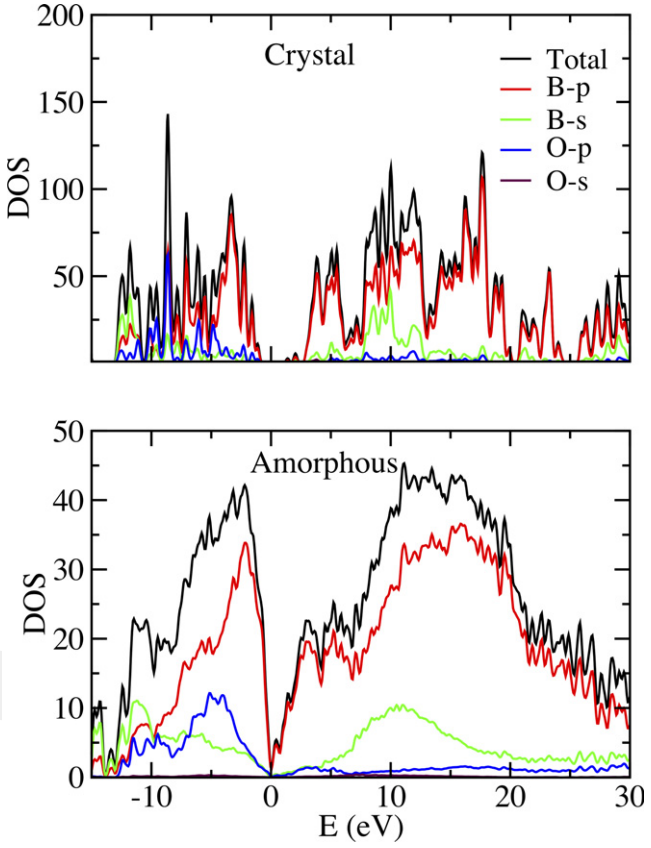

FIGURE 6 Total electron density of states (TDOS) and partial density of state (PDOS) [Color figure can be viewed at wileyonlinelibrary.com]

conduction bands, especially near the Fermi level. Yet B-s states have some contribution to the conduction band while O-p states have some contribution to the valence band. These findings are consistent with the previous simulations.[50,51]

The projected IPR is illustrated in Figure 7. The conduction tail states can be considered as localized states because they present high IPR values whereas the valence tail states are softly localized because they show low IPR values. We can realize an asymmetric localization of the band tail states and use it to distinct n-type and p-type doping for a-B_6O.[49,53] The localization of the conduction tail states might indicate that the shifting the Fermi level to the conduction band would be harder than the shifting it to the valance band and thus the p-type doping is more appropriate than n-type doping for a-B_6O.

3.3 | Mechanical properties

We first compute the energy (E)-volume (V) relation for the amorphous and crystalline phases using a variable cell optimization technique and present them in Figure 8. In order to estimate their bulk modulus (K), and equilibrium volume (V_0) and energy (E_0), we fit the E-V data the third-order Birch-Murnaghan equation of states (EOS),

$$E(V) = E_0 + \frac{9V_0K}{16}\left\{\left[\left(\frac{V_0}{V}\right)^{\frac{2}{3}} - 1\right]^3 K' + \left[\left(\frac{V_0}{V}\right)^{\frac{2}{3}} - 1\right]^2\left[6 - 4\left(\frac{V_0}{V}\right)^{\frac{2}{3}}\right]\right\}.$$

As understood from the Figure, the crystalline phase is energetically more favorable than the amorphous one as expected. From the fitting, the relative energy difference between the amorphous and crystalline structures is estimated to be about 0.35 eV/atom, signifying a high-energy barrier between them. The equilibrium volume of the crystal and noncrystalline phases is 7.64 and 9.62 Å^3/atom, respectively. Therefore, the crystal shows more compact arrangement than the amorphous network. The K value for the crystal is projected to be 231 GPa, which reasonably agrees with the other results of 230-232 GPa[51,54,55] while it is computed to be ~106 GPa for the glassy B_6O.

Since the Poisson's ratio (ν) can be simply calculated from the lateral strain ($\varepsilon_{lateral}$)—applied strain ($\varepsilon_{applied}$) relation,

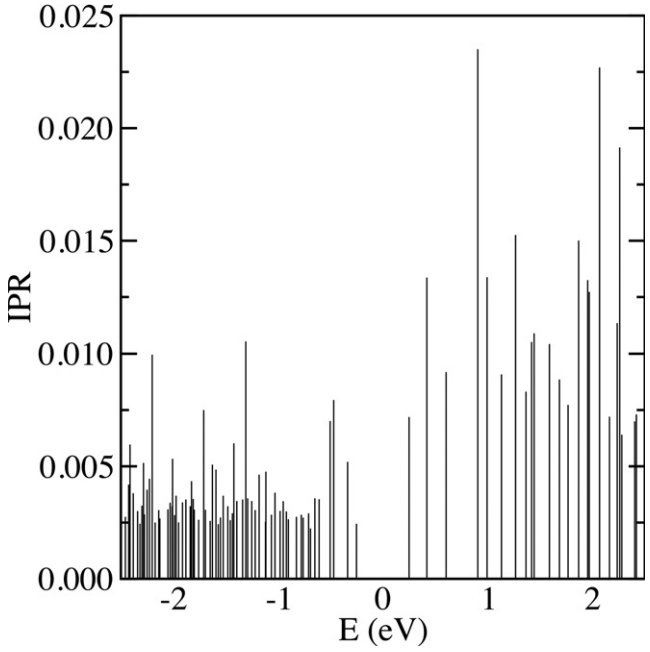

FIGURE 7 Inverse participation ratio

$$\nu = -\frac{\varepsilon_{\text{lateral}}}{\varepsilon_{\text{applied}}},$$

We compress uniaxially the simulation box along one direction, set the other stress components to zero and estimate both the lateral strain ($\varepsilon_{\text{lateral}}$)—applied strain ($\varepsilon$applied) for each applied stress. The calculations are carried out for the three principle axes and six values are obtained. Some of our data for the applied lateral strain relation of the amorphous model are provided in Figure 9. From the linear fitting, we estimate the average the Poisson's ratio to be ~0.14 for the crystal and ~0.18 for the amorphous state. For the crystalline state, our estimation pretty agrees with the earlier predictions of 0.147-0.15.[43,56]

Since two elastic constants (K and ν) are known, using the following equation,

$$E = 3K(1 - 2\nu).$$

We determine the Young modulus to be 498 GPa for the crystal and 203 GPa for the amorphous phases. Again our estimation for the crystal is parallel to the values of 480-482 GPa[43,56] reported in previous investigations.

We calculate the shear modulus (μ) using the following definition,

$$\mu = \frac{E}{2(1+\nu)}.$$

Shear modulus of the B_6O crystal is projected to be 227 GPa, agreeing with the available results of 207-218 GPa[34,43,51,54–57] in the literature. For the amorphous state the modulus is computed to be 86 GPa.

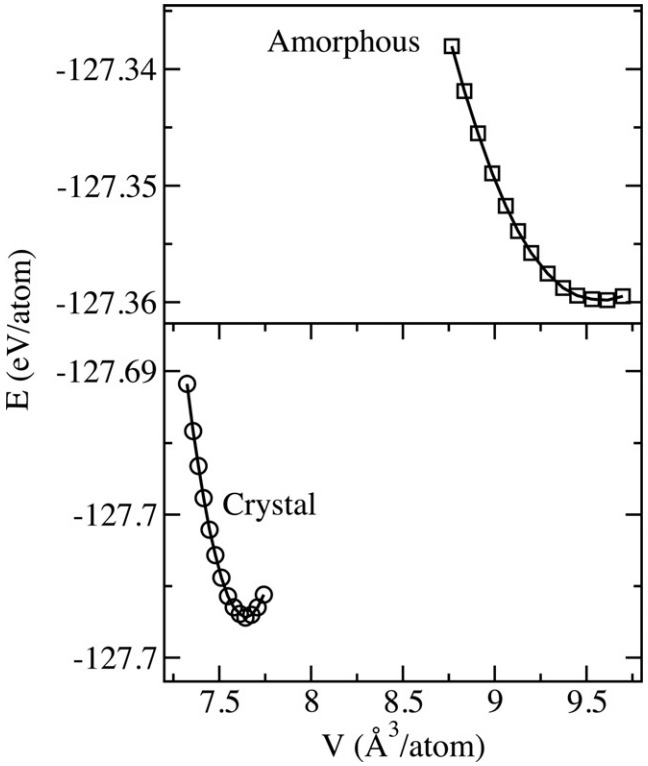

FIGURE 8 Energy-volume relation of a-B_6O and B_6O crystal

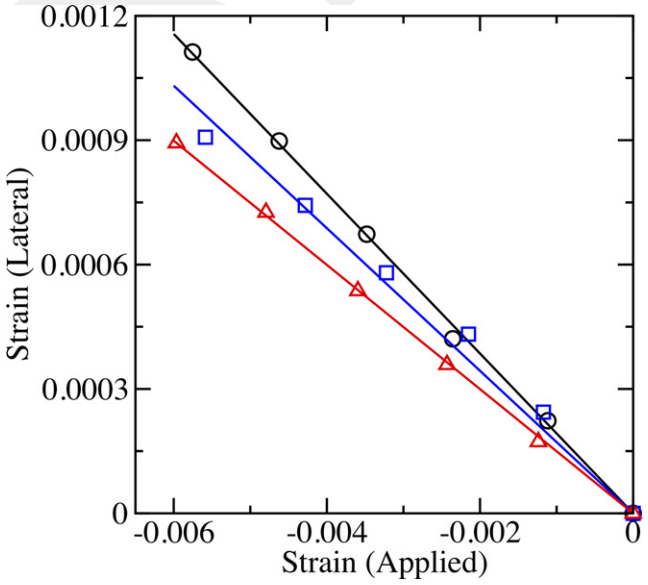

FIGURE 9 The lateral strain ($\varepsilon_{\text{lateral}}$)—applied strain ($\varepsilon_{\text{applied}}$) relation [Color figure can be viewed at wileyonlinelibrary.com]

The Vickers hardness (H_v) is another important mechanical property of materials. Considerable efforts have been devoted to resolve the relationship between H_v and elastic properties. These efforts have proven the influence of shear and bulk modules on H_v and offered some empirical relations. The first equation was proposed by Teter and indicates a linear relation between H_v and μ as follows,[58]

$$H_v = 0.151\mu.$$

The second equation suggested by Chen[59] shows a non-linear equation

$$H_v = 2\left(\frac{\mu}{n^2}\right)^{0.585} - 3(\text{GPa}),$$

where $n = K/\mu$ is called as the Pugh's ratio. Later, the Chen's equation was revised by Tian et al[60] since it leads to negative values for materials having small H_v values. The improved version of this equation is given by,

$$H_v = 0.92\left(\frac{1}{n}\right)^{1.137}(\mu)^{0.708}.$$

Form these three equations, the Vickers hardness is projected to be about 34 GPa (Teter), 43 GPa (Chen), and 41 GPa (Tian) for the crystal structure, comparable with the experimental predictions of 38-45 GPa.[7–9,34,43,51,54–,57] For the amorphous phase, on the other hand, we compute the Vickers hardness to be 13 GPa (Teter), 18 GPa (Chen) and 17 GPa (Tian). So one can see a dramatic decrease in the Vickers hardness by amorphization of B_6O.

4 | DISCUSSION

Accompanied by amorphization of B_6O, we observe a severe transformation around O atoms. The mean coordination number of O atoms changes from 3 to 2.15 and the B–O and O–O separations are shortened such that their values are comparable with those of B_2O_3. The shortened B–O and O–O distances might be attributed to a decrease in the coordination number of O atoms and the tendency of the system to form O-rich regions in the amorphous model, respectively. The visualization of the systems proposes the formation of B- and O-rich regions in the hypothetical liquid and amorphous states (Figure 4). Comparable B–O and O–O separations, the bond angle distribution function, and the coordination number of O atoms with respect to those of B_2O_3 indicate that O-rich structurally similar to the B_2O_3 system. For the B-rich regions, on the other hand, the first three-peak position of the B–B correlation is quite analogous to those of a-B. Consequently, we suggest that B-rich regions show structurally characteristics of a-B. These observations do indeed accord with the high-pressure experiment in which an amorphous state consisting of a-B and a-B_2O_3 was observed during the pressure release.[32]

The presence of such phase separations requires thermodynamically some long-range diffusion of B and O atoms. This happens in the hypothetical liquid state at 2500 K (Figure 4). Such phase separations are maintained during the fast solidification process. It should be pointed out here that at ambient pressure and temperatures, B_6O decomposes[40] but at high pressures it can be melted.[61] The experimental studies reveal that the fast quenched liquid state of B_6O at a pressure of 5.8 GPa and a temperature of 2710 ± 40 K, can lead to the formation of rhombohedral B and B_2O_3 crystals while a slow quenching rate yields the crystallization to B_6O,[61] indicating a high-energy barrier for the formation of the B_6O crystal. These observations suggest possible phase separations in the liquid phase of B_6O at high pressure(s) as well and hence support our findings.

The amorphization causes a dramatic volume expansion in B_6O. The physical origin of the volume swelling is mainly associated with the formation of open structured B_2O_3-like structure. We believe that the open structured regions are responsible for the dramatic change (softening) in the elastic properties of a-B_6O as well, relative to the B_6O crystal. Nonetheless the Vickers hardness of a-B_6O is still high and thus it can be classified as a hard material.

Another fascinating observation is the development of a B_7 molecule in a-B_6O. The formation of such a molecule, the best of our knowledge, has not been observed in boron-based amorphous and crystalline materials including a-B. Yet the B_7H_7 type cluster can be experimentally synthesized.[62] What favors the formation of the B_7 molecule is not clear but the presence of a phase separation might be responsible for it.

Finally we have to underline here that all predictions of the present work are based on a pure stoichiometric 224 atoms model. Depending on the preparation techniques, O deficiency, impurities etc. a-B_6O can be fabricated with distinctive local structure and hence different mechanical and electronic properties.

5 | CONCLUSIONS

A detailed analysis of the structural arrangements, electronic characters, and mechanical properties of a-B_6O has been carried out using an AIMD technique. The amorphous model is generated from the rapid solidification of the hypothetical melt of B_6O at ambient pressure and consists of B- and O-rich regions. The B-rich regions show the features of a-B while the O-rich regions present the characteristics of B_2O_3. In the B-rich domains, the formation of complete and incomplete B_{12} molecules is perceived. In addition to the B_{12} molecules, we also perceive the development of a pentagonal bipyramid (B_7) molecule. The amorphous phase has a rather small band gap energy relative to the crystal. The p-type doping is recommended to be more suitable than the n-type doping in a-B_6O due to the localized conduction tail states. The bulk modulus and Vicker's hardness are noticeably decreased by amorphization, which is attributed to the construction of open structured B_2O_3 domains.

ACKNOWLEDGMENTS

The present work was supported by the Scientific and Technological Research Council of Turkey (TÜBİTAK) under grant number 117M372. The simulations were run on the TÜBİTAK ULAKBİM, High Performance and Grid Computing Center (TRUBA resources).

ORCID

Murat Durandurdu https://orcid.org/0000-0001-5636-3183

REFERENCES

1. Lundstro T, Andreev YG. Superhard boron-rich borides and studies of the BCN system. Mater Sci Eng A. 1996;209:16–22.
2. Hubert H, Devouard B, Garvie LA, O'keeffe M, Buseck PR, Petuskey WT, et al. Icosahedral packing of B_{12} icosahedra in boron suboxide (B_6O). Nature. 1998;391:376–8.
3. Hubert H, Garvie LA, Devouard B, Buseck PR, Petuskey WT, McMillan PF. High-pressure, high-temperature synthesis and characterization of boron suboxide (B_6O). Chem Mater. 1998;10:1530–7.
4. Werheit H, Kuhlmann U. FTIR and FT Raman spectra of B_6O. J Solid State Chem. 1997;133:260–3.
5. He D, Zhao Y, Daemen L, Qian J, Shen TD, Zerda TW. Boron suboxide: as hard as cubic boron nitride. Appl Phys Lett. 2002; 81:643–5.
6. He D, Akaishi M, Scott BL, Zhao Y. Growth of boron suboxide crystals in the B-B_2O_3 system at high pressure and high temperature. J Mater Res. 2002;17:284–90.
7. Herrmann M, Sigalas I, Thiele M, Müller MM, Kleebe HJ, Michaelis A. Boron suboxide ultrahard materials. Int J Refract Metals Hard Mater. 2013;39:53–60.
8. Petrak RR, Ruh R, Atkins GR. Mechanical properties of hot-pressed boron suboxide and boron. Ceram Bull. 1974;53:569–73.
9. Srikanth V, Roy R, Graham EK, Voigt DE. B_xO: phases present at high pressure and temperature. J Am Ceram Soc. 1991;74:3145–7.
10. Sasai R, Fukatsu H, Kojima T, Itoh H. High pressure consolidation of B_6O-diamond mixtures. J Mater Sci. 2001;36:5339–43.
11. Itoh H, Maekawa I, Iwahara H. Microstructure and mechanical properties of B_6O-B_4C sintered composites prepared under high pressure. J Mater Sci. 2000;35:693–8.
12. Rizzo HF, Simmons WC, Bielstein HO. The existence and formation of the solid B_6O. J Electrochem Soc. 1962;109:1079–82.
13. Shabalala TC, McLachlan DS, Sigalas I, Herrmann M. Hard and tough boron suboxide based composites. Ceram Int. 2008;34: 1713–7.
14. Jiao X, Jin H, Liu F, Ding Z, Yang B, Lu F, et al. Synthesis of boron suboxide (B_6O) with ball milled boron oxide (B_2O_3) under lower pressure and temperature. J Solid State Chem. 2010;183: 1697–703.
15. Olofsson M, Lundström T. Synthesis and structure of non-stoichiometric B_6O. J Alloys Compd. 1997;257:91–5.
16. Kobayashi M, Higashi I, Brodhag C, Thevenot F. Structure of B_6O boron-suboxide by Rietveld refinement. J Mater Sci. 1993;28:2129–34.
17. Holcombe CE Jr, Horne OJ Jr. Preparation of boron suboxide, B_7O. J Am Ceram Soc. 1972;55:106.
18. Holcombe CE Jr, Horne OJ Jr, inventors; US Atomic Energy Commission (AEC), assignee. Method for preparing boron suboxide. United States patent US 3,660,031. 1972 May 2.
19. Hubert H, Garvie LA, Leinenweber K, Buseck PR, Petuskeyt WT, McMillan PF. High-pressure, high-temperature synthesis of superhard boron suboxide. MRS Online Proc Library Arch. 1995;410:191–6.
20. Itoh H, Maeka WA, Iwahara H. High pressure sintering of B_6O powder and properties of sintered compact. J Soc Mater Sci Japan. 1998;47:1000–5.
21. McMillan PF, Hubert H, Chizmeshya A, Petuskey WT, Garvie LA, Devouard B. Nucleation and growth of icosahedral boron suboxide clusters at high pressure. J Solid State Chem. 1999;147:281–90.
22. Nieto-Sanz D, Loubeyre P, Crichton W, Mezouar M. X-ray study of the synthesis of boron oxides at high pressure: phase diagram and equation of state. Phys Rev B. 2004;70:214108–14.
23. Solozhenko VL, Kurakevych OO, Bouvier P. First and second-order Raman scattering of B_6O. J Raman Spectrosc. 2009;2009 (40):1078–81.
24. Music D, Schneider JM, Kugler V, Nakao S, Jin P, Östblom M, et al. Synthesis and mechanical properties of boron suboxide thin films. J Vac Sci Technol A. 2002;20:335–7.
25. Music D, Kreissig U, Chirita V, Schneider JM, Helmersson U. Elastic modulus of amorphous boron suboxide thin films studied by theoretical and experimental methods. J Appl Phys. 2003;93:940–4.
26. Music D, Kugler VM, Czigány Z, Flink A, Werner O, Schneider JM, et al. Role of carbon in boron suboxide thin films. J Vac Sci Technol A. 2003;21:1355–8.
27. Music D, Kreissig U, Czigány ZS, Helmersson U, Schneider JM. Elastic modulus-density relationship for amorphous boron suboxide thin films. Appl Phys A. 2003;76:269–71.
28. Doughty C, Gorbatkin SM, Tsui TY, Pharr GM, Medlin DL. Hard boron–suboxide-based films deposited in a sputter-sourced, high-density plasma deposition system. J Vac Sci Technol A. 1997;15:2623–6.
29. Gorbatkin SM, Rhoades RL, Tsui TY, Oliver WC. Hard boron oxide thin-film deposition using electron cyclotron resonance microwave plasmas. Appl Phys Lett. 1994;65:2672–4.
30. Klepper CC, Hazelton RC, Yadlowsky EJ, Carlson EP, Keitz MD, Williams JM, et al. Amorphous boron coatings produced with vacuum arc deposition technology. J Vac Sci Technol A. 2002;20:725–32.
31. Music D, Schneider JM. Elastic properties of amorphous boron suboxide based solids studied using ab initio molecular dynamics. J Phys Condens Matter. 2008;20:195203–7.
32. Wang Z, Zhao Y, Lazor P, Annersten H, Saxena SK. In situ pressure Raman spectroscopy and mechanical stability of superhard boron suboxide. Appl Phys Lett. 2005;86:041911–3.
33. Reddy KM, Hirata A, Liu P, Fujita T, Goto T, Chen MW. Shear amorphization of boron suboxide. Scripta Mater. 2014;76:9–12.
34. Kunka C, An Q, Rudawski N, Subhash G, Zheng J, Halls V, et al. Nanotwinning and amorphization of boron suboxide. Acta Mater. 2018;147:195–202.

35. Ordejón P, Artacho E, Soler JM. Self-consistent order-N density-functional calculations for very large systems. Phys Rev B. 1996;53:R10441–4.
36. Troullier N, Martins JL. Efficient pseudopotentials for plane-wave calculations. Phys Rev B. 1991;43:1993–2006.
37. Becke AD. Density functional exchange energy approximation with correct asymptotic behavior. Phys Rev A. 1988;38:3098–100.
38. Lee C, Yang W, Parr RG. Development of the Colle-Salvetti correlation-energy formula into a functional of the electron density. Phys Rev B. 1988;37:785–9.
39. Parrinello M, Rahman A. Polymorphic transitions in single crystals: a new molecular dynamics method. J Appl Phys. 1981;52:7182–90.
40. Rizzo HF, Simmons WC, Bielstein HO. The existence and formation of the solid B_6O. J Electrochem Soc. 1962;109(11):1079–82.
41. Le Roux S, Petkov V. ISAACS—interactive structure analysis of amorphous and crystalline systems. J Appl Crystallogr. 2010;43:181–5.
42. Momma K, Izumi F. VESTA 3 for three-dimensional visualization of crystal, volumetric and morphology data. J Appl Crystallogr. 2011;44:1272–6.
43. Rahane AB, Kumar V, Dunn JS. Carbon doping in boron suboxide: structure, energetics, and elastic properties. J Am Ceram Soc. 2015;98:2223–33.
44. Lundström T. Structure and bulk modulus of high-strength boron compounds. J Solid State Chem. 1997;133:88–92.
45. Delaplane RG, Dahlborg U, Howells WS, Lundström T. A neutron diffraction study of amorphous boron using a pulsed source. J Non Cryst Solids. 1988;106(1–3):66–9.
46. Krishnan S, Ansell S, Felten JJ, Volin KJ, Price DL. Structure of liquid boron. Phys Rev Lett. 1998;81:586–9.
47. Durandurdu M. Liquid boron and amorphous boron: an ab initio molecular dynamics study. J Non Cryst Solids. 2015;417:10–4.
48. Medvedev NN. The algorithm for three-dimensional Voronoi polyhedral. J Comput Phys. 1986;67:223–9.
49. Cai B, Drabold DA. Properties of amorphous GaN from first-principles simulations. Phys Rev B. 2011;84:075216–21.
50. Li D, Ching WY. Electronic structure and optical properties of the $B_{12}O_2$ crystal. Phys Rev B. 1996;54:1451–4.
51. Wang J, Wang Z, Jing Y, Wang S, Chou CF, Hu H, et al. Electronic structure and optical properties of boron suboxide B_6O system: first-principles investigations. Solid State Commun. 2016;244:12–6.
52. Varley JB, Lordi V, Miglio A, Hautier G. Electronic structure and defect properties of B_6O from hybrid functional and many-body perturbation theory calculations: a possible ambipolar transparent conductor. Phys Rev B. 2014;90:045205–13.
53. Robertson J. Physics of amorphous conducting oxides. J Non Cryst Solids. 2008;354:2791–5.
54. Zhang RF, Lin ZJ, Zhao YS, Veprek S. Superhard materials with low elastic moduli: three-dimensional covalent bonding as the origin of superhardness in B_6O. Phys Rev B. 2011;83:092101–4.
55. An Q, Reddy KM, Dong H, Chen MW, Oganov AR, Goddard WA III. Nanotwinned boron suboxide (B_6O): new ground state of B_6O. Nano Lett. 2016;16(7):4236–42.
56. Wang Y, Wang Y, Yao T, Li H, Wu L, Yang M, et al. Metallization and softening of B6O at high pressure. J Alloys Compd. 2014;600:71–7.
57. Dong H, Oganov AR, Wang Q, Wang SN, Wang Z, Zhang J, et al. Prediction of a new ground state of superhard compound B_6O at ambient conditions. Sci Rep. 2016;6:31288–94.
58. Teter DM. Computational alchemy: the search for new superhard materials. MRS Bull. 1998;23:22–7.
59. Chen XQ, Niu H, Li D, Li Y. Modeling hardness of polycrystalline materials and bulk metallic glasses. Intermetallics. 2011;19:1275–81.
60. Tian Y, Xu B, Zhao Z. Microscopic theory of hardness and design of novel superhard crystals. Int J Refract Met Hard Mater. 2012;33:93–106.
61. Solozhenko VL, Lathe C. On the melting temperature of B_6O. J Superhard Mater. 2007;29(4):259–60.
62. Schlüter F, Bernhardt E. Syntheses and crystal structures of the closo-borates $M_2[B_7H_7]$ and $M[B_7H_8]$(M= PPh_4, PNP, and N (n-Bu_4)): the missing crystal structure in the series $[B_nH_n]^{2-}$ (n = 6–12). Inorg Chem. 2011;50:2580–9.

How to cite this article: Durandurdu M. Amorphous boron suboxide. *J Am Ceram Soc*. 2019;102:4546–4554. https://doi.org/10.1111/jace.16324